# Cortical cell stiffness is independent of substrate mechanics

Johannes Rheinlaender[1,†,*], Andrea Dimitracopoulos[1], Bernhard Wallmeyer[2], Nils M. Kronenberg[3], Kevin J. Chalut[4], Malte C. Gather[3], Timo Betz[2], Guillaume Charras[5,6], and Kristian Franze[1]*

[1] Department of Physiology, Development and Neuroscience, University of Cambridge, Cambridge, UK.

[2] Centre for Molecular Biology of Inflammation, Institute of Cell Biology, Excellence cluster Cells in Motion, University of Münster, Münster, Germany

[3] SUPA, School of Physics and Astronomy, University of St Andrews, St Andrews KY16 9SS, UK

[4] Wellcome Trust-Medical Research Council Cambridge Stem Cell Institute, University of Cambridge, Cambridge, UK

[5] London Centre for Nanotechnology, University College London, 17-19 Gordon Street, London, UK.

[6] Department of Cell and Developmental Biology, University College London, Gower Street, London, UK

[†] Present address: Institute of Applied Physics, University of Tübingen, Auf der Morgenstelle 10, 72076 Tübingen, Germany.

[*] To whom correspondence should be addressed: johannes.rheinlaender@uni-tuebingen.de
kf284@cam.ac.uk

Keywords: cell stiffness, stiffening, AFM, substrate stiffness, polyacrylamide, ERISM

## ABSTRACT

**Cell stiffness is a key cellular material property that changes locally and temporally during many cellular functions including migration, adhesion, and growth. Currently, it is widely accepted that cells adapt their mechanical properties to the stiffness of their surroundings. The link between cortical cell stiffness and substrate mechanics was hypothesized based on atomic force microscopy (AFM) indentation measurements of cells cultured on deformable substrates. Here we show that the force applied by AFM can result in a significant deformation not only of the cell surface but also of the underlying substrate if it is sufficiently soft. This 'soft substrate effect' leads to an underestimation of a cell's elastic modulus on substrates softer than the cells when fitting the indentation data using a standard Hertz model, as confirmed by finite element modelling (FEM) and AFM measurements of calibrated polyacrylamide beads, microglial cells, and fibroblasts. To account for this substrate deformation, we developed the 'composite cell-substrate model' ('CoCS' model), which does not require any knowledge about the cell-substrate geometry, and which can be implemented in any standard AFM indentation measurement. Our results provide a new formalism to analyze indentation data obtained for cells cultured on soft matrices, and they suggest that cortical cell stiffness is largely independent of substrate mechanics, which has significant implications for our interpretation of many physiological and pathological processes.**

*In vivo*, cells respond to the mechanical properties of their environment[1,2]. As the stiffness of any tissue critically depends on the mechanical properties of its constituent cells, cell mechanics measurements are key to understanding many complex biological processes. Over the last decades, atomic force microscopy (AFM) has emerged as a gold standard to assess the mechanical properties of cells[3-6]. In AFM measurements, a force is applied perpendicular to the cell surface, and the resulting deformation is used to calculate an apparent elastic modulus, which is a measure of the cell's stiffness. Depending on the force applied, different cellular structures contribute differently to the measured elastic moduli[6]. AFM indentation measurements of cells using low stresses (force per area) and thus resulting in small strains (relative deformations) mainly probe peripheral cellular structures including the actomyosin cortex[7] and the pericellular coat[8], and the contribution of other factors such as membrane tension, hydrostatic pressure, and cell organelles is rather minor. The measured apparent elastic moduli can then be interpreted as an effective cortical cell stiffness.

Previous AFM studies suggested that the cortical stiffness of cells increases with increasing substrate stiffness[9-13]. The application of blebbistatin, which blocks myosin II function and thus cell contractility, abolished the apparent stiffening of the cells on stiffer substrates. Hence, it was hypothesized that, as cells increase their traction forces on stiffer substrates, the increased pre-stress of the actomyosin network leads to its non-linear stress stiffening and accordingly to an overall stiffening of the cells[9].

In AFM indentation measurements, the relation between the loading force $F$ and the overall sample indentation $\delta$ is mostly modeled using the Hertz model[14], which in the case of a spherical probe is as follows:

$$F(\delta) = \frac{4}{3}\frac{E_{\text{cell}}}{1-\nu_{\text{cell}}^2}\sqrt{r}\cdot\delta^{3/2} \approx \frac{16}{9}E_{\text{cell}}\sqrt{r}\cdot\delta^{3/2} \quad , \tag{1}$$

where $r$ is the probe radius, $\nu_{\text{cell}}$ is the cell's Poisson's ratio, which usually is close to $\nu_{\text{cell}}\sim 0.5$[15,16], and $E_{\text{cell}}$ is the apparent elastic modulus of the cell. The only quantities recorded during an experiment are the cantilever's vertical displacement $\Delta z$ and its deflection $d$. $d$ is used to calculate the applied force $F = k \cdot d$, where $k$ is the cantilever's spring constant. The indentation depth $\delta = \Delta z - d$ is inferred from these quantities based on the key assumption that the sample is deformed but not the underlying substrate (Figure 1a). However, while this condition is clearly fulfilled for cells cultured on glass or tissue culture plastics, it may no longer

hold for cells cultured on soft matrices mimicking the mechanical properties of the physiological cell environment[17].

Indeed, when we cultured microglial cells on polyacrylamide substrates with stiffnesses ranging from $E_{\mathrm{substrate}} = 50$ Pa to 20 kPa and probed them by AFM, we noticed that the force exerted on the cells led to substantial deformations of the polyacrylamide substrate, in contradiction with analytical assumptions (Figure 1, see **Error! Reference source not found.** for details). To quantify this substrate deformation, we combined AFM with confocal laser scanning microscopy. On stiffer substrates ($E_{\mathrm{substrate}} \approx 2$ kPa), the force applied by the cantilever on the cells resulted in negligible vertical displacements of the substrate (Figure 1a). On softer substrates ($E_{\mathrm{substrate}} \approx 100$ Pa), however, the applied force resulted in a significant vertical displacement of the substrates on the order of 1 µm (Figure 1b). Moreover, the substrate displacement depended linearly on the loading force (Figure 1c and d, $\bar{R}^2 \geq 0.998$), with a small apparent deformability $c = \delta_{\mathrm{substrate}}/F$ of around 0.1 µm/nN for stiff substrates (Figure 1c) and a significantly larger deformability of $c \sim 0.9$ µm/nN for soft substrates (Figure 1d) (see also **Error! Reference source not found.**g-i and **Error! Reference source not found.**e).

These experiments suggested that the indentation $\delta$ inferred from AFM measurements is actually the sum of the indentation of the cell $\delta_{\mathrm{cell}}$ and that of the underlying deformable substrate $\delta_{\mathrm{substrate}}$, signifying that $\Delta z - d = \delta_{\mathrm{cell}} + \delta_{\mathrm{substrate}}$ (Figure 1e). On hard substrates, $\delta_{\mathrm{substrate}}$ is negligible and $\delta_{\mathrm{cell}}$ can be directly inferred from the measurements as usually done. However, on soft substrates, excluding $\delta_{\mathrm{substrate}}$ would lead to an overestimation of $\delta_{\mathrm{cell}}$ and thus to an underestimation of the cell's apparent elastic modulus $E_{\mathrm{cell}}$ when using the standard Hertz model, Equation (1). In other words, if the substrate underneath a cell is deformed during an AFM measurement, the Hertz model's boundary condition that the substrate is not moving at the 'infinite' border is not valid (the whole reference frame of the cell is moving), and hence the Hertz model cannot be applied without an appropriate correction.

To address this challenge, we first considered a simple analytical model to characterize the deformation of an elastic cell in contact with a deformable substrate, similar to having two elastic springs in series (Figure 1f). The loading force applied by the cantilever onto the cell is balanced by the elastic deformation of the substrate underneath the cell (i.e., the force experienced by the substrate is the same as that exerted on the cell).

To investigate the vertical displacement field of the substrate under cells caused by AFM indentation measurements in more detail, we combined AFM with Elastic Resonator Interference Stress Microscopy (ERISM)[18,19], which quantifies the vertical deformation of deformable substrates with high spatial resolution (Figure 2). Both the substrate deformation and the stress were maximum under the cell center, where the cantilever was located, and increased linearly with the applied force (Figure 2a). Substrate deformation and stress also decayed approximately linearly away from the cell center until reaching zero ~10 µm away from the cantilever (Figure 2b). The shape of the substrate deformation and stress distribution did not vary for different applied forces.

We therefore assumed an axisymmetric stress distribution with maximum stress of $\sigma_0$ below the cell center and linear decrease from the center to zero within a distance, approximated by the cell radius $R$ (Figure 2c). The substrate deformation can then be approximated by the elastic response of a semi-infinite half space due to axisymmetric stress distribution on a circular region[20], also known as the Boussinesq solution[21]:

$$\delta_{\text{substrate}} \cong \frac{1-\nu_{\text{substrate}}^2}{E_{\text{substrate}}} R \cdot \sigma_0 = \frac{9}{4\pi} \frac{F}{R\, E_{\text{substrate}}} \quad , \tag{2}$$

(Figure 2c) where $\nu_{\text{substrate}} = 0.5$ for polyacrylamide gels[22]. Note that the cell-substrate contact results in a linear force-indentation relation. As the maximum stress linearly increased with the applied force but its functional form remained unaltered (Figure 2b), the force-indentation relation will be linear also for any arbitrary cell morphologies.

In contrast, the indentation of the cell follows the non-linear Hertz model[14]:

$$F = \frac{16}{9} E_{\text{cell}} \sqrt{r} \cdot \delta_{\text{cell}}^{3/2} \quad . \tag{3}$$

The measured overall indentation $\delta$ is then a combination of the indentation of the cell and that of the substrate,

$$\delta = \delta_{\text{cell}} + \delta_{\text{substrate}} \quad . \tag{4}$$

Rearranging Equation (3) and inserting it with Equation (2) into Equation (4) gives the relation between the measured overall indentation and the applied loading force

$$\delta(F) = a \cdot F^b + c \cdot F \tag{5}$$

with the pre-factor $a = \left(16/9 \cdot E_{\text{cell}} \cdot \sqrt{r}\right)^{-2/3}$, the exponent $b = 2/3$, and

$$c \cong \frac{9}{4\pi} \frac{1}{R\, E_{\text{substrate}}} \approx \frac{1}{R\, E_{\text{substrate}}} \quad , \tag{6}$$

which is proportional to the inverse of the substrate stiffness. $c$ can be interpreted as the effective substrate deformability, *i.e.*, a measure of how much the substrate is deformed during a measurement. In reality, the cell bottom will also deform to some degree. Hence, the measured deformability will have contributions from the deformation of both the substrate and the cell bottom. Note that this analytical model can easily be adapted to other Poisson's ratios or tip geometries (for example for conical/pyramidal tips using $b = 1/2$ and a different relation for $a$ according to the respective contact model[23,24]), and that the tip geometry only affects $\delta_{\text{cell}}$.

Since the terms accounting for a cell's elastic modulus (non-linear Hertz contact) and substrate deformability (linear contact) are linearly independent, fitting Equation (5) to the inverse relationship between force and indentation, with $a$ and $c$ as free parameters, allows the determination of the cell's elastic modulus and the substrate deformability independently of each other. We termed this approach the 'composite cell-substrate model' ('CoCS model').

To test the effect of substrate stiffness on the measured cell stiffness in AFM experiments, we first used a finite element model (FEM) to generate ground-truth force-distance curves for different ratios of $E_{\text{substrate}}/E_{\text{cell}}$ and different indenter geometries (Figure 3a and b, see Methods and **Error! Reference source not found.** and **Error! Reference source not found.** for details). We chose a half-spherical geometry to represent the cell (Figure 1a, b).

When we fit the simulated force distance curves with the Hertz model, the calculated values of $E_{\text{cell}}$ matched the actual values only on stiff but not on soft substrates, where the cells appeared much softer than they were (0.1 $E_{\text{cell}}$; Figure 3c, lower trace) and the analytical fit deviated from the simulated curves (Figure 3c, arrow; $\bar{R}^2 = 0.949$ for soft *vs.* 0.999 for stiff substrates). Moreover, while on stiff substrates the force distance curves always followed the expected $\delta^{3/2}$-dependency of the Hertz contact, on soft substrates they followed the $\delta^{3/2}$-dependency only for small forces but approached a linear $\delta$-dependency for large forces due to the increasing influence of the substrate deformation (**Error! Reference source not found.**b).

In contrast, fitting Equation (5) to the same data plotted as indentation *vs.* force (Figure 3d) returned correct mechanical properties of the cells irrespective of substrate stiffness. The

measured cell elastic moduli were now similar on soft and stiff substrates and close to the actual values (here 1.07 $E_{\mathrm{cell}}$ on stiff and 1.06 $E_{\mathrm{cell}}$ on soft substrates; Fig. 3d), and the analytical fits matched the simulated curves very well ($\bar{R}^2 \geq 0.999$). In addition to the real cell elastic moduli, the fits also returned the substrate deformability. As assumed by the analytical model (see above), the substrate deformation linearly depended on the loading force, and this was well-predicted from the CoCS model fit (**Error! Reference source not found.**c).

We then used FEM to simulate force-distance curves for a large range of substrate stiffnesses (Figure 3e). Performing the CoCS model fit [Eq. (5)] on the simulated force-indentation data indeed yielded the cell elastic moduli correctly and independently of the substrate stiffness (Figure 3e, blue trace). In contrast, the classic Hertz model fit (Figure 3e, red trace) provided the correct cell stiffness only when the substrate stiffness was large compared to the cell stiffness, $E_{\mathrm{substrate}}/E_{\mathrm{cell}} \gg 1$, and it significantly underestimated the cell stiffness when it was comparable to or larger than the substrate stiffness, $E_{\mathrm{substrate}}/E_{\mathrm{cell}} \lesssim 1$. Similar results were obtained for other tip shapes (**Error! Reference source not found.**) and other cell sizes and shapes such as more spherical or well-spread shapes (**Error! Reference source not found.**).

To test whether the new analysis can accurately determine the stiffness of a real sample with known properties supported by a deformable substrate, we prepared elastic polyacrylamide beads of similar diameters as cells (but significantly larger diameters than cantilever probes) and with a typical stiffness of $E_{\mathrm{bead}} \cong 1 - 2$ kPa. These beads were bound to polyacrylamide substrates of different stiffnesses (see Methods) and force indentation curves acquired by AFM. Polyacrylamide is a homogeneous, isotropic, and linearly elastic material. Thus, the mechanical properties of the beads should be independent of the properties of the substrate.

On stiff substrates ($E_{\mathrm{substrate}} \approx 10$ kPa), the force *vs.* indentation data was fit well with the standard Hertz model (Figure 4a), and the indentation *vs.* force data was fit well with the CoCS model (Figure 4b). On soft substrates ($E_{\mathrm{substrate}} \approx 1$ kPa), however, the standard Hertz fit strongly deviated from the experimental force indentation curves ($\bar{R}^2 = 0.962$ *vs.* 0.999 on stiff substrates) (Figure 4c), whereas the CoCS model fit always matched well with the data ($\bar{R}^2 \geq 0.999$) (Figure 4d). Overall, the CoCS model fit the experimental data significantly better than the Hertz model on soft substrates, while both models performed similarly well on stiff substrates (**Error! Reference source not found.**a).

The substrate deformability derived from the CoCS model was significantly larger for the soft substrate ($c = 51 \pm 7$ nm/nN, average $\pm$ SEM) compared to the stiff substrates ($c = 7.2 \pm 1.1$ nm/nN) (Figure 4e), where the substrate deformation was negligible, indicating that part of the measured overall indentation on soft but not on stiff substrates was due to the indentation of the substrate by the polyacrylamide beads. As a side note, the substrate deformability $c$ directly depends on the substrate's elastic modulus, as predicted by the analytical model, Equation (6), and by FEM (Figure 3e). Hence, $c$ can also be used to estimate the substrate's elastic modulus $E_{\text{substrate}} \approx 1/(Rc)$, obtained by rearranging Equation (6). Using a typical contact radius $R \approx 20$ µm (see Figure 4a, c), our experiments yielded elastic moduli of $E_{\text{substrate}} \approx 1.0 \pm 0.1$ kPa for the soft and $7 \pm 1$ kPa for the stiff substrates, in reasonable agreement with the actual substrate elastic moduli measured directly of $1.4 \pm 0.1$ kPa and $9 \pm 2$ kPa, respectively (Figure 4e).

While on stiff substrates both fits yielded similar elastic moduli for the beads of around ~1.2 kPa, on soft substrates the Hertz fit predicted a significantly lower average $E_{\text{bead}} = 0.7$ kPa compared to the CoCS model fit and compared to the stiffness determined for beads on the stiff substrates (Figure 4f, red). In contrast, the CoCS model fit (Figure 4f, blue) estimated bead elastic moduli of around ~1.2 kPa regardless of the substrate stiffness, as expected given that the beads were made of the same material. Together, these data confirmed that our new approach can be used to accurately analyze the elastic stiffness of a sample irrespective of the stiffness of the underlying substrate, in contrast to the commonly used Hertz model.

Having validated the ability of our new approach to accurately determine the stiffness of samples regardless of substrate stiffness, we sought to determine if cells indeed adjusted their stiffness to that of their environment[9-13] or if the reported increase in cell stiffness observed on stiffer substrates might be the result of an underestimation of the cells' elastic moduli on soft substrates due to fitting of force-indentation curves with the Hertz model (Figs. 3e, 4f). As in the bead experiments (Figure 4), analytical fits using the Hertz model deviated considerably from the experimental force-distance curves for primary microglial cells cultured on soft matrices (Figure 5b, $\bar{R}^2 = 0.970$) whereas this was not the case when the cells were cultured on stiff substrates (Figure 5a, $\bar{R}^2 = 0.997$). In contrast, the analytical solution for the CoCS model fitted both conditions equally well (Figure 5c, d; $\bar{R}^2 \geq 0.995$). Again, overall the CoCS model fit the

experimental data significantly better than the Hertz model on soft and intermediate substrates, while they worked similarly well on stiff substrates (**Error! Reference source not found.**b).

A quantitative analysis using the CoCS model revealed that the measured apparent deformability of the substrates significantly increased with decreasing substrate stiffness (Figure 5e), indicating that a significant part of the overall indentation measured when applying forces to cells cultured on soft substrates originated from the deformation of the substrate.

When analyzed using the standard Hertz model, apparent elastic moduli of microglial cells $E_{\mathrm{cell}}$ decreased significantly from an average ~100 Pa on stiffer substrates to ~40 Pa on soft substrates (Figure 5f), consistent with previous reports for other cell types[9-13] (see also Figure 6). In contrast, the CoCS model (Figure 5f, blue bars) yielded significantly larger apparent elastic moduli than the Hertz model for soft and intermediate substrate stiffnesses, but similar moduli on stiff substrates. Moreover, when analyzed with the CoCS model, cell moduli did not depend on substrate stiffness, remaining around 100 Pa on all substrates (Figure 5f). These results suggested that the overall stiffness of microglial cells is independent of substrate stiffness, similarly to that of polyacrylamide beads.

To test if the observed behavior is specific to microglial cells or a more general phenomenon, we repeated these experiments with fibroblasts, which have previously been suggested to adapt their stiffness to that of their environment[9]. As in our microglia experiments, fibroblasts only showed the apparent softening on softer substrates when using standard Hertz fits, but did not show any significant changes in stiffness when analyzed using the CoCS model (**Error! Reference source not found.**). Together, these data suggested that cells do not adapt their overall mechanical properties to substrate stiffness.

In previous reports, perturbations of actomyosin contractility were shown to prevent the apparent stiffening of cells on stiffer substrates[25-27]. When we treated cells with the myosin II inhibitor blebbistatin, elastic moduli of microglial cells significantly decreased by about 20% (**Error! Reference source not found.**). The measured apparent elastic moduli did not depend on the substrate stiffness or on the fit model (Figure 5h). Indeed, as the ratio of $E_{\mathrm{substrate}}/E_{\mathrm{cell}}$ significantly increased, the substrates were significantly less deformed by the indented cells and hence the substrate deformability was similar across all different substrates (Figure 5g) and generally smaller than without blebbistatin (Figure 5e). These results suggested that blebbistatin reduced the overall cortical stiffness of the cells, and the deformation of the softened cells was

consequently much larger than that of the underlying stiffer substrate. Thus, blebbistatin treatment increased the accuracy of the Hertz model because it decreased substrate indentation by the softened cell.

While this softening of cells after blebbistatin treatment (Fig. 5 and Supplementary Fig. 8) suggested a significant contribution of the actomyosin cortex to the measured apparent elastic moduli, some cells possess an extensive pericellular coat, which can affect the estimation of the cortical cell stiffness measured by AFM[8,16,28]. To investigate the predictions of the CoCS model for samples exhibiting a pericellular coat at their surface, we first extended the FEM simulations by adding a layer representing a pericellular coat. Regardless of whether the layer was softer or stiffer than the cell, the CoCS model fit yielded the cell stiffness independently of substrate stiffness, while the Hertz fit again underestimated the cell stiffness for soft substrates (**Error! Reference source not found.**a, b). Furthermore, we functionalized PAA beads with a polyethylene glycol (PEG) layer mimicking a pericellular coat (**Error! Reference source not found.**c; see Methods). As for the uncoated beads (Figure 4) and FEM simulations, elastic moduli were independent of substrate stiffness when using the CoCS model fit but correlated with substrate stiffness when using standard Hertz fits (**Error! Reference source not found.**e, f). Taken together, the CoCS model is reliable also when applied to cells with a pericellular coat.

## Discussion

Given that it is established that cell function is critically regulated by substrate mechanics[29-33], soft substrates mimicking the mechanical properties of the physiological cell environment are widely used. Cell stiffness measurements on these substrates are crucial to understanding mechanical interactions of cells with their environment. However, measurements of cortical cell stiffness on deformable substrates are challenging, and current suggested correction methods to account for substrate mechanical properties are rather complex[34,35]. Here we show that, in AFM indentation measurements, the force exerted on a cell is transmitted to the soft substrate underneath, causing its deformation (Figure 1). The Hertz model, which is commonly used to analyze indentation experiments of soft biological materials, underestimates cortical cell stiffness on soft substrates but converges towards the correct apparent elastic moduli on progressively stiffer substrates (Figs. 3-6).

To account for this 'soft substrate effect', we here present a straightforward approach for estimating the apparent elastic moduli of cells on deformable substrates from AFM force-indentation curves, which can be applied without any prior knowledge of cell morphology (**Error! Reference source not found.**) or the need for hardware modifications. Motivated by simple analytical considerations, we used ground-truth data from numerical simulations and experimental data from soft elastic polyacrylamide beads on polyacrylamide substrates to validate our method, which we term the 'composite cell-substrate model' ('CoCS' model). The CoCS model reliably returned the correct values for all samples independently of substrate stiffness (Figs. 4, 5, Supplementary Figs. 7, 8, 10) and indentation depth $\delta$ (Supplementary Fig. 6), confirming self-consistency of the CoCS model.

Cell stiffness characterizes the resistance of cells to deformation in response to forces. In case of small externally applied forces, the deformation is largely determined by peripheral cellular structures. Blebbistatin significantly reduced the apparent elastic modulus of the cells (Figs. 5h, S8), indicating that the actin cortex is a major contributor to the cortical stiffness measured in our experiments. Thick pericellular brushes found in some cell types will also contribute to apparent elastic moduli measured by AFM[14,21,22]. The CoCS model works well also for cells with pericellular coats, returning moduli independent of substrate stiffness (Fig. **Error! Reference source not found.**), and it can be combined in the future with other models[36] to disentangle the contributions of the coat and the cells to the measurements.

Cortical cell stiffness is cell type-specific, may depend on chemical signaling[37], and change during pathological processes such as cancer metastasis[38]. Similar to chemical signals, mechanical signals may impact cell behavior *in vitro* as well as *in vivo*[1,2]. For example, an increase in substrate stiffness leads to an increase in cellular traction forces and in cell spreading[39,40] (**Error! Reference source not found.**). Previous reports using a Hertz model-based analysis of AFM indentation data also suggested that the stiffness of cells cultured on soft polyacrylamide gels first increases with increasing substrate stiffness and then plateaus. This behavior has been described for a variety of cell types including fibroblasts[9], human mesenchymal stem cells[10], aortic valve interstitial cells[11], thyroid cells[12], and cardiac myocytes[13].

We made similar observations when analyzing our own AFM data using the Hertz model (Figure 6a). However, when correcting for the 'soft substrate effect' using the CoCS model, elastic moduli of both polyacrylamide beads and the cells remained largely constant and

independent of substrate stiffness. Substrate stiffness might have a similarly small effect on the cortical stiffness of other cell types (*cf.* Figure 6a).

Microglial cells and fibroblasts spread more and exert higher traction forces as the substrate's stiffness increases[41-43], as confirmed in our study (**Error! Reference source not found.**a-h). The current conceptual model explaining cortical cell stiffness sensitivity to substrate mechanics hypothesizes that, as actomyosin-based contractile (traction) forces of cells increase with increasing substrate stiffness, the actin cortex stress-stiffens on stiffer substrates, leading to a substrate mechanics-dependent stiffening of the cell as a whole[9-13,25-27,29-32,44]. However, traction forces in two-dimensional cultures are mainly generated by ventral stress fibers[45] rather than by the cortical actin network. While it is likely that stress fibers are at least partly coupled to the actin cortex, the lack of cortical cell stiffening in AFM indentation measurements of cells cultured on stiffer substrates (Figure 5 and **Error! Reference source not found.**) suggests that these forces are dissipated with increasing distance from the stress fibres (Figure 6b).

In both previous studies and our current work, Hertz model fits did not return any significant (apparent) stiffening of cells on stiffer substrates when myosin II was blocked by blebbistatin. These findings were explained by the loss of contractility-driven stress stiffening of the actin cortex[10,25-27]. However, blebbistatin blocks myosin II in a detached state[46], and in this way reduces the cross-linking of the whole actin cortex. As a consequence of the reduced cross-linking, the overall elastic modulus of the actin cortex is decreased irrespective of contractile forces. The resulting global softening of the actin cortex after blebbistatin application (Figure 5) leads to an increase in the $E_{\mathrm{substrate}}/E_{\mathrm{cell}}$ ratio, which significantly reduces the 'soft substrate effect' (Figure 3e) observed when analyzing the data with Hertz fits. Hence, the cellular indentation $\delta_{\mathrm{cell}} = \Delta z - d$ is correctly determined in those experiments and the Hertz model no longer underestimates the apparent elastic modulus of the cells, thus providing an alternative explanation of why blebbistatin-treated cells do not seem to 'soften' on softer substrates (Figure 5f).

When cells are cultured on stiff substrates, substrate effects in AFM measurements can be avoided by limiting the indentation depth to less than ~10% of the sample height[47,48]. Importantly, this is not the case when cells are grown on soft substrates. In our simulations as well as in the experiments, indentations did not exceed 10% of the sample (cell or bead) height, and yet the sample stiffness was underestimated on soft gels (Figure 3e and Figure 4f).

Depending on the ratio of $E_{\mathrm{substrate}}/E_{\mathrm{sample}}$, samples may be pushed into the substrate even at very low forces / small indentations, suggesting that this effect cannot be experimentally avoided when using AFM or any other nanoindentation approaches. However, our model provides a straight-forward tool to correct for this 'soft substrate effect', thus enabling AFM-based cell mechanics measurements on substrates with physiologically relevant stiffnesses. It is also likely applicable to cells invading a soft substrate[35,49] and to cells in an *in situ* environment within soft biological tissues (for example metastatic cancer), thus significantly widening the scope and accuracy of AFM-based cell stiffness measurements.

## References


1 Koser, D. E. *et al.* Mechanosensing is critical for axon growth in the developing brain. *Nat. Neurosci.* **19**, 1592, (2016).

2 Barriga, E. H., Franze, K., Charras, G. & Mayor, R. Tissue stiffening coordinates morphogenesis by triggering collective cell migration in vivo. *Nature* **554**, 523–527, (2018).

3 Haase, K. & Pelling, A. E. Investigating cell mechanics with atomic force microscopy. *J. R. Soc. Interface* **12**, 20140970, (2015).

4 Gautier, H. O. B. *et al.* in *Methods in Cell Biology* Vol. 125 (ed Ewa K. Paluch) 211-235 (Academic Press, 2015).

5 Dufrêne, Y. F. *et al.* Imaging modes of atomic force microscopy for application in molecular and cell biology. *Nat. Nanotechnol.* **12**, 295-307, (2017).

6 Wu, P.-H. *et al.* A comparison of methods to assess cell mechanical properties. *Nat. Methods* **15**, 491-498, (2018).

7 Vahabikashi, A. *et al.* Probe Sensitivity to Cortical versus Intracellular Cytoskeletal Network Stiffness. *Biophys. J.* **116**, 518-529, (2019).

8 Iyer, S., Gaikwad, R. M., Subba-Rao, V., Woodworth, C. D. & Sokolov, I. Atomic force microscopy detects differences in the surface brush of normal and cancerous cells. *Nat. Nanotechnol.* **4**, 389, (2009).

9 Solon, J., Levental, I., Sengupta, K., Georges, P. C. & Janmey, P. A. Fibroblast Adaptation and Stiffness Matching to Soft Elastic Substrates. *Biophys. J.* **93**, 4453-4461, (2007).

10 Tee, S.-Y., Fu, J., Chen, Christopher S. & Janmey, Paul A. Cell Shape and Substrate Rigidity Both Regulate Cell Stiffness. *Biophys. J.* **100**, L25-L27, (2011).

11 Liu, H., Sun, Y. & Simmons, C. A. Determination of local and global elastic moduli of valve interstitial cells cultured on soft substrates. *Journal of Biomechanics* **46**, 1967-1971, (2013).

12 Rianna, C. & Radmacher, M. Comparison of viscoelastic properties of cancer and normal thyroid cells on different stiffness substrates. *Eur. Biophys. J.* **46**, 309-324, (2017).

13 Chopra, A., Tabdanov, E., Patel, H., Janmey, P. A. & Kresh, J. Y. Cardiac myocyte remodeling mediated by N-cadherin-dependent mechanosensing. *American journal of physiology* **300**, H1252-1266, (2011).

14 Hertz, H. Über die Berührung fester elastischer Körper. *J. Reine Angew. Math.* **92**, 156-171, (1882).

15 Harris, A. R. & Charras, G. T. Experimental validation of atomic force microscopy-based cell elasticity measurements. *Nanotechnology* **22**, 345102, (2011).

16 Guz, N., Dokukin, M., Kalaparthi, V. & Sokolov, I. If Cell Mechanics Can Be Described by Elastic Modulus: Study of Different Models and Probes Used in Indentation Experiments. *Biophys. J.* **107**, 564-575, (2014).

17 Ivanovska, I. L. *et al.* Cross-linked matrix rigidity and soluble retinoids synergize in nuclear lamina regulation of stem cell differentiation. *Mol. Biol. Cell* **28**, 2010-2022, (2017).

18 Kronenberg, N. M. *et al.* Long-term imaging of cellular forces with high precision by elastic resonator interference stress microscopy. *Nat. Cell Biol.* **19**, 864, (2017).

19 Liehm, P., Kronenberg, N. M. & Gather, M. C. Analysis of the Precision, Robustness, and Speed of Elastic Resonator Interference Stress Microscopy. *Biophys. J.* **114**, 2180-2193, (2018).

20 Johnson, K. L. *Contact Mechanics*. (Cambridge University Press, 1985).

21 Boussinesq, J. Application des potentiels à l'étude de l'équilibre et du mouvement des solides élastiques, principalement au calcul des déformations et des pressions que produisent, dans ces solides, des efforts quelconques exercés sur une petite partie de leur surface ou de leur intérieur : mémoire suivi de notes étendues sur divers points de physique mathématique et d'analyse. (Impr. L. Danel ( Lille ), 1885).

22 Boudou, T., Ohayon, J., Picart, C. & Tracqui, P. An extended relationship for the characterization of Young's modulus and Poisson's ratio of tunable polyacrylamide gels. *Biorheology* **43**, 721-728, (2006).

23 Sneddon, I. N. The relation between load and penetration in the axisymmetric boussinesq problem for a punch of arbitrary profile. *Int. J. Eng. Sci.* **3**, 47-57, (1965).
24 Bilodeau, G. G. Regular pyramid punch problem. *J. Appl. Mech.* **59**, 519-523, (1992).
25 Chrzanowska-Wodnicka, M. & Burridge, K. Rho-stimulated contractility drives the formation of stress fibers and focal adhesions. *J. Cell Biol.* **133**, 1403-1415, (1996).
26 Pelham, R. J. & Wang, Y.-l. Cell locomotion and focal adhesions are regulated by substrate flexibility. *Proc. Natl. Acad. Sci. U.S.A.* **94**, 13661-13665, (1997).
27 Engler, A. J. *et al.* Myotubes differentiate optimally on substrates with tissue-like stiffness. *J. Cell Biol.* **166**, 877-887, (2004).
28 Simon, M. *et al.* Load Rate and Temperature Dependent Mechanical Properties of the Cortical Neuron and Its Pericellular Layer Measured by Atomic Force Microscopy. *Langmuir* **32**, 1111-1119, (2016).
29 Chen, C. S., Mrksich, M., Huang, S., Whitesides, G. M. & Ingber, D. E. Geometric Control of Cell Life and Death. *Science* **276**, 1425-1428, (1997).
30 Discher, D. E., Janmey, P. A. & Wang, Y. Tissue cells feel and respond to the stiffness of their substrate. *Science* **310**, 1139-1143, (2005).
31 Engler, A. J., Sen, S., Sweeney, H. L. & Discher, D. E. Matrix elasticity directs stem cell lineage specification. *Cell* **126**, 677-689, (2006).
32 Gupta, M. *et al.* Adaptive rheology and ordering of cell cytoskeleton govern matrix rigidity sensing. *Nat. Commun.* **6**, 7525, (2015).
33 Segel, M. *et al.* Niche stiffness underlies the ageing of central nervous system progenitor cells. *Nature* **573**, 130-134, (2019).
34 Vichare, S., Sen, S. & Inamdar, M. M. Cellular mechanoadaptation to substrate mechanical properties: contributions of substrate stiffness and thickness to cell stiffness measurements using AFM. *Soft Matter* **10**, 1174-1181, (2014).
35 Staunton, J. R., Doss, B. L., Lindsay, S. & Ros, R. Correlating confocal microscopy and atomic force indentation reveals metastatic cancer cells stiffen during invasion into collagen I matrices. *Sci. Rep.* **6**, 19686, (2016).
36 Krieg, M. *et al.* Atomic force microscopy-based mechanobiology. *Nat. Rev. Phys.* **1**, 41-57, (2019).
37 Pogoda, K. *et al.* Soft Substrates Containing Hyaluronan Mimic the Effects of Increased Stiffness on Morphology, Motility, and Proliferation of Glioma Cells. *Biomacromolecules* **18**, 3040-3051, (2017).
38 Cross, S. E., Jin, Y. S., Rao, J. & Gimzewski, J. K. Nanomechanical analysis of cells from cancer patients. *Nature nanotechnology* **2**, 780-783, (2007).
39 Discher, D. E., Janmey, P. & Wang, Y. L. Tissue cells feel and respond to the stiffness of their substrate. *Science* **310**, 1139-1143, (2005).
40 Yeung, T. *et al.* Effects of substrate stiffness on cell morphology, cytoskeletal structure, and adhesion. *Cell Motil Cytoskeleton* **60**, 24-34, (2005).
41 Bollmann, L. *et al.* Microglia mechanics: immune activation alters traction forces and durotaxis. *Front. Cell. Neurosci.* **9**, (2015).
42 Han, S. J., Bielawski, K. S., Ting, L. H., Rodriguez, M. L. & Sniadecki, N. J. Decoupling substrate stiffness, spread area, and micropost density: a close spatial relationship between traction forces and focal adhesions. *Biophys J* **103**, 640-648, (2012).
43 Moshayedi, P. *et al.* The relationship between glial cell mechanosensitivity and foreign body reactions in the central nervous system. *Biomaterials* **35**, 3919-3925, (2014).
44 Kasza, K. E. *et al.* The cell as a material. *Current Opinion in Cell Biology* **19**, 101-107, (2007).
45 Soine, J. R. *et al.* Model-based traction force microscopy reveals differential tension in cellular actin bundles. *PLoS computational biology* **11**, e1004076, (2015).
46 Kovacs, M., Toth, J., Hetenyi, C., Malnasi-Csizmadia, A. & Sellers, J. R. Mechanism of blebbistatin inhibition of myosin II. *J Biol Chem* **279**, 35557-35563, (2004).
47 Dimitriadis, E. K., Horkay, F., Maresca, J., Kachar, B. & Chadwick, R. S. Determination of elastic moduli of thin layers of soft material using the atomic force microscope. *Biophys. J.* **82**, 2798-2810, (2002).

48 Charras, G. T., Lehenkari, P. P. & Horton, M. A. Atomic force microscopy can be used to mechanically stimulate osteoblasts and evaluate cellular strain distributions. *Ultramicroscopy* **86**, 85-95, (2001).
49 Kristal-Muscal, R., Dvir, L. & Weihs, D. Metastatic cancer cells tenaciously indent impenetrable, soft substrates. *New J. Phys.* **15**, 035022, (2013).
50 Moshayedi, P. *et al.* Mechanosensitivity of astrocytes on optimized polyacrylamide gels analyzed by quantitative morphometry. *J. Phys.: Condens. Matter* **22**, 194114, (2010).
51 Wilby, M. J. *et al.* N-Cadherin Inhibits Schwann Cell Migration on Astrocytes. *Mol. Cell. Neurosci.* **14**, 66-84, (1999).
52 Cook, S. M. *et al.* Practical implementation of dynamic methods for measuring atomic force microscope cantilever spring constants. *Nanotechnology* **17**, 2135-2145, (2006).
53 Gavara, N. Combined strategies for optimal detection of the contact point in AFM force-indentation curves obtained on thin samples and adherent cells. *Sci. Rep.* **6**, 21267, (2016).
54 Han, S. J., Oak, Y., Groisman, A. & Danuser, G. Traction microscopy to identify force modulation in subresolution adhesions. *Nat. Methods* **12**, 653, (2015).
55 McGill, R., Tukey, J. W. & Larsen, W. A. Variations of Box Plots. *The American Statistician* **32**, 12-16, (1978).

## Acknowledgements

The authors would like to thank Paul Janmey, Ben Fabry, Ulrich Schwarz, and Manuel Thery for critical discussions and comments on the manuscript, Lars Bollmann for traction force microscopy images, and Alex Winkel (JPK) for technical support. NIH3T3 cells were a kind gift from William Colledge. We acknowledge funding from the German Science Foundation (DFG grant RH 147/1-1 to J.R., EXC 1003 CiM to T.B.), the Herchel Smith Foundation (postdoctoral fellowship to A.D.), the UK EPSRC (Programme grant EP/P030017/1 to M.C.G.), the European Research Council (Consolidator Grants 771201 to T.B., 647186 to G.C., and 772426 to K.F.), the Human Frontier Science Program (HFSP grant RGP0018/2017 to T.B.), the UK BBSRC (Equipment grant BB/R000042/1 to G.C., and Research Project grant BB/N006402/1 to K.F.).

## Author contributions

J.R. and K.F. conceived the study; J.R. conducted all AFM experiments, analyzed all AFM data and developed the model, A.D. conducted all optical imaging and traction force microscopy experiments and analyzed data, B.W. and T.B. custom-designed polyacrylamide beads, N.M.K. and M.C.G. conducted ERISM measurements, K.J.C. helped with imaging and data analysis, G.C. helped with AFM experiments, all authors discussed the study, J.R. and K.F. wrote the paper with contributions from all co-authors.

## Data and code availability

The data underlying this study are available from the authors upon reasonable request. Codes used for processing of AFM and confocal laser scanning microscopy raw data can be found at https://github.com/FranzeLab/AFM-data-analysis-and-processing/tree/master/Cell%20stiffness

## Additional information

Supplementary information is available in the online version of the paper.

## Competing financial interests

The authors declare no competing financial interests.

## Methods

**Substrate preparation.** Deformable PAA gel substrates as described previously [1,43,50]. Briefly, cover slips were glued into custom-made petri dishes, cleaned and silanized with (3-aminopropyl)trimethoxysilane (APTMS; unless otherwise stated, all chemicals from Sigma-Aldrich, Dorset, UK) for 3 min (minutes), treated with glutaraldehyde (diluted 1:10) for 30 min. Gel premixes were made by thoroughly mixing 440 µL of 40% acrylamide, 60 µL of 100% hydroxyl-acrylamide, and 250 µL of 2% Bis-acrylamide. The premix was then mixed with PBS at ratios between 40 µL to 460 µL and 150 µL to 350 µL to achieve gel stiffness between 50 Pa and 20 kPa. Polymerization was initialized by adding 0.3% (v/v) N,N,N′,N′-tetramethylethylenediamine (TEMED) and 0.1% (w/v) ammonium persulfate (APS) and 20 µL of the solution (giving about 100 µm gel thickness) were covered with cover slips, which were made hydrophobic with RainX (Shell Car Care International Ltd, UK) for 10 min beforehand. After at least 20 min top cover slips were removed, washed 2x with PBS, sterilized under UV light for 30 min, functionalized with either 100 µg/mL poly-D-lysine overnight for microglia cells or with 0.2 mg/mL fibronectin (FC010, Merck, 1:5 in PBS) for 2h at 37°C for fibroblasts, and washed 2x with PBS.

**PAA bead preparation.** An AH-mix was produced by mixing 100 µL of 40% acrylamide with 13 µL of 97 % N-Hydroxyethyl acrylamide. Then, 50 µL of 2% Bis-acrylamide were added to 100 µL of AH-mix (ABH-mix). For the pre-bead-solution, first 100 µL of ABH-mix and 325 µL of PBS were mixed. This mixture was degassed for 10 min before adding 75 µL of 10% APS. The pH value of the pre-bead-solution was neutralized by adding 2.25 µL of 6M NaOH. An emulsion was generated by injecting 50 µL of pre-bead-solution in 500 µL of n-hexane with 3% Span®80 (Sigma-Aldrich) using a 100 µL Hamilton Syringe. After discarding the supernatant, the polymerization of the emulsion was initialized by adding 1.5 µL TEMED and keeping the emulsion at 85 °C for 10 min. After polymerization was finished, the beads were washed with n-hexane and transferred into 500 µL PBS. The elastic PAA beads were fluorescently labeled by preparing an ATTO488-solution of 1 mg ATTO 488 NHS-Ester (ATTO-TEC) in 200 µL Dimethylsulfoxide and adding 6 µL ATTO488-solution to the PAA beads in PBS. After 3 hours, the PAA beads were washed by centrifugation at a relative centrifugal force of 600 for 5 min. The supernatant was discarded and replaced by fresh PBS. The labeling and washing procedure

was repeated three times. PAA beads were immobilized on the gel substrates by coating the substrates for 2 h with Cell-Tak (Corning Cat No 354240, 1:25 in PBS) and incubating the bead solution overnight at 4°C. By monitoring the beads in fluorescence microscopy during the AFM measurement it was ensured that beads were rigidly bound to the substrate. The strong adhesion resulted in a finite contact area between bead and substrate rather than a point contact (Figure 4a and c, insets), making the bead-substrate contact analogous to a cell adhered a substrate, although the beads did not have a half-spherical shape. To investigate the influence of a pericellular coat on cell stiffness measurements, PAA beads were functionalized with a PEG layer. Beads where prepared similar as described above, however, instead of the ABH mix, a mixture of 100 µL of 40% acrylamide 50 µL of 2% Bis-acrylamide and 0.8 µL of Acylic-Acid (Sigma Aldrich, Germany) was generated (ABA-mix). For the PEG coating a 20kDa PEG polymer with NH2 and COOH groups on either end was used (NH2-PEG20K-COOH, Sigma-Aldrich, Germany). The NH2 side of the PEG polymer was bound to the beads by first activating the carboxyl groups exposed on the surface of the beads via ECD/NHS, allowing efficient covalent binding of the PEG. The still exposed COOH group of the PEG polymer allows to create multiple layers of the PEG coating. Here we performed this step 3 times to get an effective length of 60kDa. Briefly, an activation mixture was prepared using 1 ml of a NaCL/MES mix (solving 195mg MES, 4-Morpholineethanesulfonic acid, and 292 mg NaCl in 10ml pure water), which was added to 0.05 g EDC (*N*-(3-Dimethylaminopropyl)-*N*′-ethylcarbodiimide, Sigma-Aldrich, Germany). The coating was done in the following three step procedure: I) 1mL of the resulting solution was added to 11.5 mg NHS (N-Hydroxysuccinimide, Sigma-Aldrich, Germany) and vortexed. 500mL of this activation mix was added to the beads solution (500µL) and incubated for 15 minutes at room temperature. II) Immediately afterwards the beads where washed with PBS, and after a final centrifugation, 125mL of PBS was added after discarding the supernatant. 30µL of a NH2-PEG20K-COOH stock solution (500mg of NH2-PEG20K-COOH in 2500µL pure water) was added to the washed beads and incubated at room temperature. III) Finally, the beads where washed with PBS and filled up to 500µL total volume. The steps I)-III) where repeated three times.

**Culture preparation.** Primary microglial cells were prepared from neonatal rat cerebral cortices as previously described[51]. Briefly, mixed glia cultures were prepared from neonatal rat cerebral cortices and cultured until they became confluent. Microglia and oligodendrocyte

progenitor cells (OPCs) were then shaken-off at 320 rpm for 60 min and allowed to adhere for 20-25 min to uncoated culture dishes (Corning 430591), after which microglia but not OPCs adhere, which were then washed off. Fibroblasts were cultured in DMEM (with 10% FBS, 1% penicillin-streptomycin, glutamax). Microglial cells or fibroblast were then seeded on PAA substrates at a density of typically 10,000 cells/cm$^2$ and cultured overnight. AFM measurements were performed in $CO_2$-independent medium (Leibovitz L-15, w/o phenolred, with glutamax) at 37°C (using PetriDishHeater, JPK Instruments AG, Berlin, Germany). For inhibition of myosin, cells were incubated for 30 min in Leibovitz L-15 containing 20 µM blebbistatin (from stock solution 25 mM in DMSO) prior to measurements. For washout of blebbistatin, cells were washed three times and incubated for 30 min in fresh Leibovitz L-15 prior to measurement. For control measurements, 0.8 µL DMSO was added to 1mL of medium.

**Atomic force microscopy (AFM).** AFM measurements were performed on JPK Cellhesion 200 AFMs (JPK Instruments AG) installed either on a conventional (Axio Observer.A1, Carl Zeiss Ltd., Cambridge, UK) or a confocal optical microscope (see below). Tip-less AFM cantilevers (Arrow TL1, nominal spring constant $k = 0.03\,\mathrm{N/m}$, NanoWorld, Neuchâtel, Switzerland,) were calibrated using the thermal noise method[52]. Subsequently, monodisperse polystyrene micro-spheres (micro-particles GmbH, Berlin, Germany) with diameter $2r = 5$ µm (PS/Q-R-KM153, Figure 5) or 10 µm (Figure 4) without or with fluorescence (diameter 5 µm, PS-FluoRed-Fi300, Figure 1) where then glued to cantilevers (M-Bond 610, Micro-Measurements, Raleigh, NC, USA, agent and adhesive mixed at 1: 1.3 weight ratio, cured at 80°C overnight). The sizes of the cantilever probes were chosen small to remain within the boundaries of the Hertz model. All AFM data was recorded with 1 kHz and subsequently filtered to 100 Hz sampling rates using binomial smoothing. For recording force *vs.* indentation data, the cantilever was positioned visually above the cell and then approached at $5\,\mu\mathrm{m/s}$ until reaching a force set point of 500 pN for microglia cells, 1.5 nN for fibroblast, and 25 nN for beads. The force set point values were chosen to maximize signal to noise ratios while avoiding an influence of the finite cell height[47,48]. As common in AFM data analysis[53], force $F$ and tip indentation $\delta$ were calculated form the cantilever deflection $d$ using the cantilever spring constant $k$ and the vertical cantilever position $z$ using $F = k \cdot (d - d_0)$ and $\delta = z - z_0 - d$, where $z_0$ and $d_0$ denote the vertical cantilever position and deflection at the point of contact of the tip with the cell, respectively. The point of contact was detected as the first point where the

force increased by threefold the standard deviation above baseline, and the force curve was fit with the respective fit model [Equations (1) and (5)] between contact point and force set point using LMA least-squares fitting. For measuring the substrate stiffness, force curves were recorded on the substrate next to the cells or beads with force set points according to the substrate stiffness to maintain a consistent maximum indentation of about 2 µm.

**Confocal laser scanning microscopy.** Combined AFM measurements and confocal microscopy were performed using a JPK Nanowizard AFM interfaced to a confocal laser scanning microscope (Olympus Fluoview FV1000, Olympus, Hamburg, Germany) equipped with a 40x silicon oil objective (NA 0.9, UPLSAPO, Olympus). For measuring the substrate displacement (Figure 1a and b), $x$-$z$ profiles were recorded through the cell center, while the cantilever was applied a constant force between 0.5 and 1.5 nN using the AFM's force feedback. The substrate displacement was calculated by comparison of the two profiles using a modified cross correlation procedure to achieve sub-resolution accuracy (see **Error! Reference source not found.** for details). For confocal fluorescence microcopy, the PAA gels were fluorescently labeled by replacing 5 µL of the PBS with 1% (w/v) fluorescein O,O′-dimethacrylate in DMSO. Cells were incubated with 20 µM CellTracker Deep Red (Thermo Fisher Scientific) in serum-free medium for 30 min.

**Elastic resonator interference stress microscopy.** ERISM substrates with an apparent stiffness of 3 kPa were fabricated as described previously.[18] A silicon chamber (surface area: 1.6 x 1.6 $cm^2$, Ibidi) was applied to the ERISM substrate and the substrate surface was functionalized by incubating 1.5 mL of type 1 collagen (Collagen A, Biochrome) at pH 3.0-3.5 for one hour at 37 °C. After functionalization, the substrate was washed with cell culture medium (DMEM w/ glutamax, 10% FCS, 1% P/S; Gibco). 3T3 fibroblasts (Sigma-Aldrich) were seeded at a density of 2,000 cells/$cm^2$ and cultured for 24 hours. AFM indentation measurements were performed with a Nanosurf FlexAFM on an inverted microscope (Nikon Ti) fitted with a heated stage. A spherical glass bead with a diameter of 12 µm was glued to a cantilever (qp-SCONT, Nanosensors) with a force constant of 0.011 N $m^{-1}$ (measured by the thermal-tuning method before attaching the bead). The cantilever deflection was calibrated by pushing the beaded cantilever against a rigid glass substrate using a known z-travel distance. Combined ERISM-AFM measurements were carried out in cell medium at 37 °C. First, maps of the vertical

substrate deformation caused by the contractility of the cell were recorded by imaging the reflectance of the ERISM substrate at 201 different wavelengths between 550 and 750 nm as described previously.[18] Next, the AFM cantilever was lowered onto the center of the cell until a compression force of 0.5 nN was reached. The force was kept constant via a feedback loop while repeating the ERISM readout using a reduced wavelength range of 51 nm to accelerate the measurement (<5 s)[19]. The compression force was successively increased to 1.0 nN and 1.5 nN, respectively, and ERISM readout was repeated for both forces. A final ERISM measurement was performed after the AFM cantilever was fully retracted again to ensure cell contractility had not changed significantly over the course of AFM indentation. The substrate displacement under the cell caused by AFM indentation was obtained by subtracting the displacement map of the cell without AFM indentation from the displacement maps taken at the different AFM indentation forces. Filtered ERISM displacement maps (Gaussian blur with 1.6 µm bandwidth) were converted into stress maps using FEM as described in [18].

**Modelling.** Finite element calculations were performed using Comsol Multiphysics 4.1 (COMSOL AB, Stockholm, Sweden). Briefly, in an axisymmetric model cell and substrate were modelled as linear-elastic with Young's modulus $E_{\mathrm{cell}}$ and $E_{\mathrm{substrate}}$, respectively, and incompressible (Poisson ratio $\nu = 0.49$), as generally assumed for living cells [15,16] and hydrogels [22]. The contact between tip and cell was modeled as friction-less and the contact between cell and substrate was modelled as a direct mechanical contact. The mesh consisted of typically $10^4$ elements. The elastic displacement of cell and substrate was then calculated in response to a tip loading force $F$ between zero and $0.5\ E_{\mathrm{cell}}\ r^2$, resulting in a maximum indentation of typically $\delta_{\mathrm{cell}} \cong 0.4r$.

**Traction force microcopy.** PAA gels were prepared on imaging dishes (µ-Dish, Ibidi, Germany) as described above. Fluorescent nanoparticles (FluoSpheres carboxylate, 0.2 µm, crimson, Life Technologies, UK) were added to the PAA pre-mixes at a concentration of 0.2 % volume and were then placed in an ultrasonic bath for 30 s to separate the beads. After starting polymerization, the imaging dish was inverted to ensure that beads settled close to the gel surface. Fibroblasts or microglia were seeded onto PAA gels with shear storage moduli G′ of 100 Pa (microglia only), 1 kPa (fibroblasts and microglia) and 10 kPa (fibroblasts only). After 24 h, cells where imaged using an inverted microscope (Leica DMi8) at 37 °C and 5% CO2, equipped

with a digital sCMOS camera (ORCA-Flash4.0, Hamamatsu Photonics), an EL6000 illuminator (Leica, Germany), and a 63× oil objective (NA1.4, Leica, Germany). Images were acquired using the Leica LAS X software. Fluorescence images of beads, and widefield images of cells were taken every 2 min. After the image acquisition, the culture media were exchanged with Trypsin-EDTA (Gibco) to detach cells from the gel. Reference images of fluorescent beads were taken 15 min after trypsinization. Traction stress maps were calculated for each frame using a TFM Software Package in MATLAB[54]. Traction stresses were averaged over time for each cell. Post-processing of the data and statistical analyses were done with a custom Python script. A detailed quantification of microglial traction forces on substrates of different stiffness can be found in a previous study[41].

**Data processing and statistical analysis.** AFM data and optical images were processed and analyzed in Igor Pro 6 (Wavemetrics, Portland, OR) using custom-written software. For measuring PAA beads and cells on substrates of different stiffness, for each bead / cell three force curves were recorded and analyzed and their median values used. Presented values represent median unless otherwise stated. Box plots show median (band), quartiles (box), and standard error of median (notches), calculated as $0.93 \times IQR/\sqrt{N}$ with $IQR$ and $N$ being inter-quartile-range and number of independent experiments, respectively.[55] Goodness of fit was quantified using the adjusted coefficient of determination, $\bar{R}^2 = 1 - (1 - R^2)\,(n-1)/(n-p-1)$, to account for the different number of fit parameters $p$ with number of data points $n$ and coefficient of determination $R^2$. As stiffness values followed log-normal distributions, statistical significance was tested using two-tailed Student's *t*-tests (for two groups), two-tailed paired Student's *t*-tests (for stiffness ratios), or one-way ANOVA followed by Tukey tests (for three or more groups) on logarithmized stiffness values. Deformability, $\bar{R}^2$, cell area, and mean traction stress values did not follow log-normal or normal distributions and were therefore tested for statistical significance using two-tailed Wilcoxon-Mann-Whitney *U* tests (for two groups) or one-way Kruskal-Wallis *H* test analysis of variance followed by Dunn-Holland-Wolfe tests (for three or more groups). Statistical significance was indicated using * for $P < 0.05$, ** for $P < 0.01$, and *** for $P < 0.001$, and "n.s." for no statistical significant difference.

# FIGURES

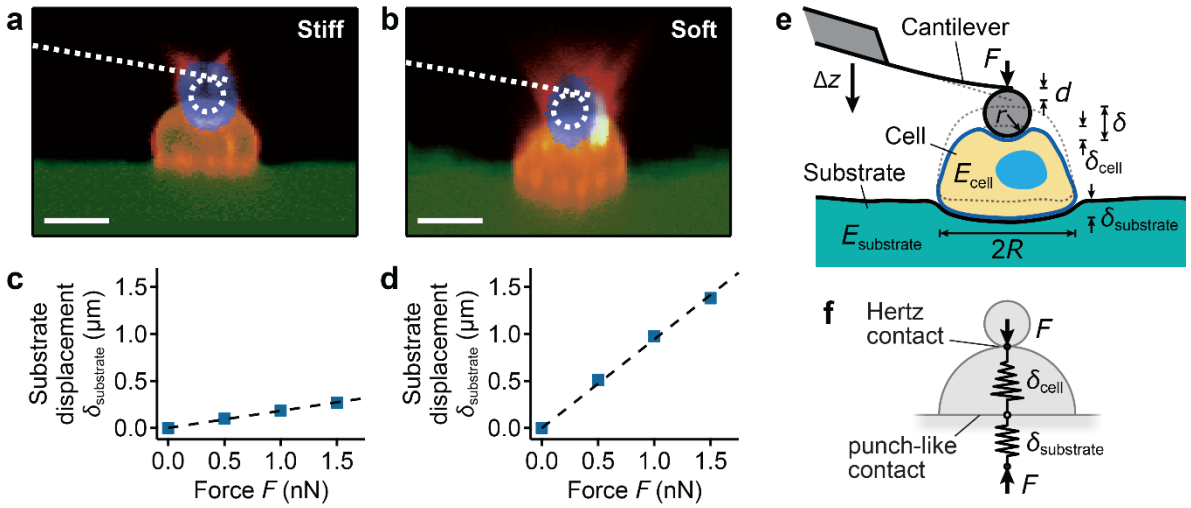


**Figure 1: Quantification of substrate displacements in AFM indentation measurements of cells. (a, b)** Confocal *z*-*x* profiles of microglial cells (orange) cultured on **(a)** stiff (≈ 2 kPa) and **(b)** soft (≈ 100 Pa) substrates (green). The AFM probe (blue) is applying a loading force of $F = 1$ nN on each cell. Scale bars: 10 µm. **(c, d)** Relationship between substrate displacements obtained from confocal images of the cells shown in **(a)** and **(b)** and the applied force $F$ on **(c)** stiff and **(d)** soft substrates (see also **Error! Reference source not found.**g-i). Forces exerted on cells by AFM indentation result in significant deformations particularly of soft substrates. **(e)** Schematic of an AFM cantilever with a spherical probe of radius $r$ pushing on a cell with elastic modulus $E_{\mathrm{cell}}$ and radius $R$ bound to a substrate with elastic modulus $E_{\mathrm{substrate}}$. The measured indentation $\delta$ is a combination of the indentation of the cell, $\delta_{\mathrm{cell}}$, and that of the substrate, $\delta_{\mathrm{substrate}}$. The dotted outline indicates the undeformed state. $\Delta z$ denotes vertical cantilever displacement, $d$ cantilever deflection. **(f)** Schematic of the mechanical system, consisting of the two springs in series, which both experience the same force. The tip-cell contact follows the nonlinear Hertz model[14], and the cell-substrate contact follows a linear force-indentation relation[20,21].

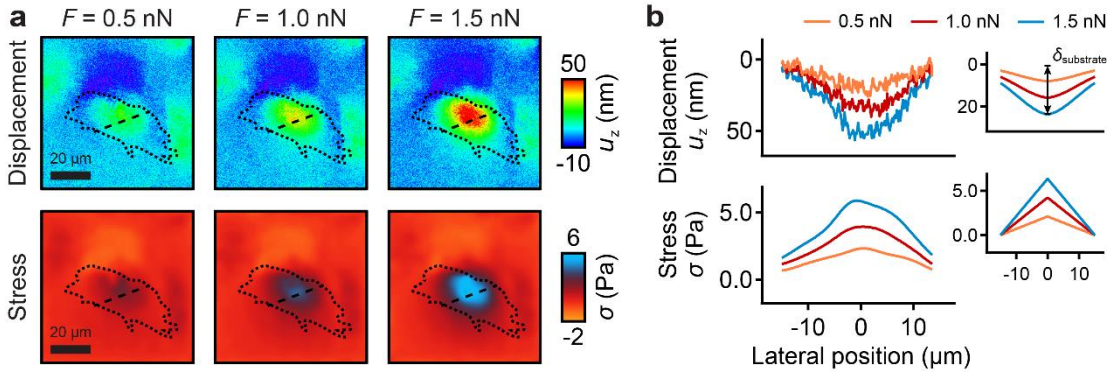


**Figure 2: Substrate displacement and stress distribution under cells caused by AFM indentation measurements. (a)** Displacement (top row) and stress distribution (bottom row) of the substrate measured by ERISM[18] at different forces $F$ applied by AFM. Dotted line: outline of the cell; dashed line: location of profiles shown in (b). **(b)** Profiles of displacement (top) and stress (bottom) under the cell shown in (a). The insets in (b) show displacement (top) and stress (bottom) predicted by the analytical model using an effective cell radius of $R = 15$ µm. There is very good qualitative and quantitative agreement between the model and the data.

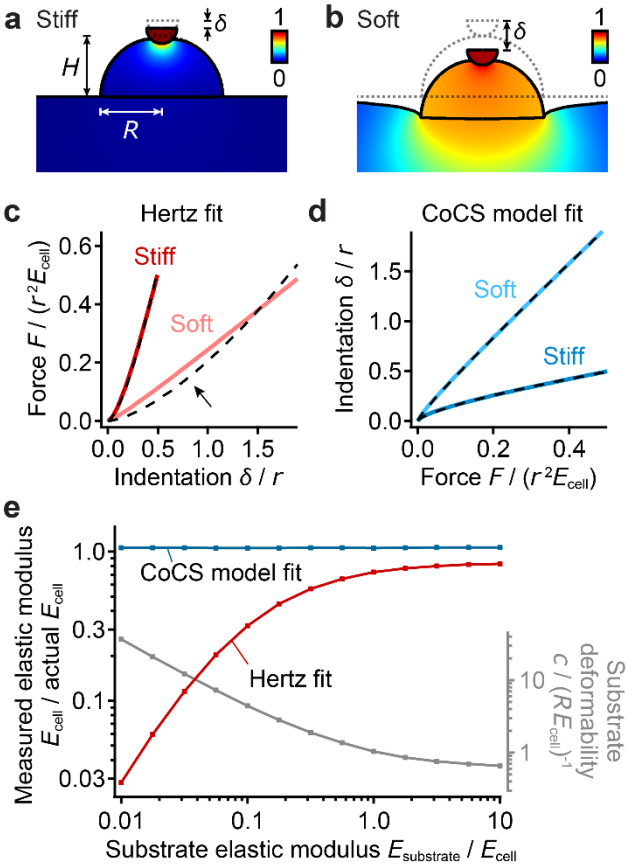


**Figure 3: Numerical validation. (a, b)** Representative FEM results for cells on **(a)** a stiff substrate and **(b)** a soft substrate for the force $F = 0.5\, r^2 E_{\mathrm{cell}}$. Color shows material displacement in units of tip displacement. $\delta$ indicates the measured total indentation relative to the undeformed state (dotted outlines). **(c)** Force $F$ *vs.* indentation $\delta$ (scaled in units of cell stiffness and tip radius) for cells on stiff and soft substrates analyzed with standard Hertz model fits, Equation (1) (dashed traces). The Hertz model deviates from the data in measurements on soft substrates (arrow). **(d)** Indentation $\delta$ *vs.* force $F$ for cells on soft and stiff substrates with CoCS model fits, Equation (5) (dashed traces). **(e)** Measured elastic moduli $E_{\mathrm{cell}}$ in units of the actual elastic moduli of the cells as a function of relative substrate stiffness as obtained fitting force-indentation curves simulated by FEM using a standard Hertz fit (Equation (1), red trace), or using the CoCS model fit (Equation (5), blue trace). Right axis shows substrate deformability obtained from the CoCS model fit. (**a-d**) Parameters of calculations shown: cell height and radius $H = R = 4r$, $E_{\mathrm{substrate}}/E_{\mathrm{cell}} = 3$ ("stiff") and $0.03$ ("soft").

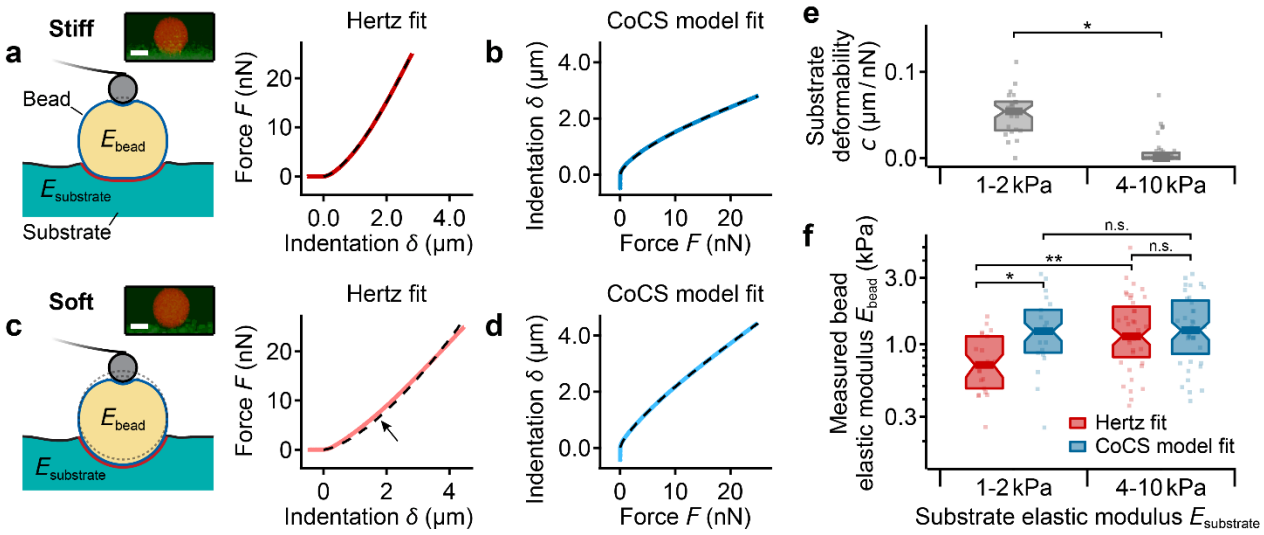


**Figure 4: Experimental validation using PAA beads. (a)** Schematic of AFM stiffness measurement of an elastic bead with stiffness $E_{\mathrm{bead}}$ on a stiff substrate ($E_{\mathrm{substrate}} \approx 10$ kPa $\gg E_{\mathrm{bead}}$) and representative measured force $F$ *vs.* indentation $\delta$ curve analyzed with standard Hertz model fit, Equation (1). The experimental data is shown by the red solid line and the fit by the dashed trace. **(b)** Same data as in **(a)**, indentation $\delta$ *vs.* force $F$ analyzed with the CoCS model fit, Equation (5) (dashed trace). **(c)** Schematic for bead on a soft substrate ($E_{\mathrm{substrate}} \approx 1$ kPa $\approx E_{\mathrm{bead}}$) and representative measured force $F$ *vs.* indentation $\delta$ curve with standard Hertz model fit, Equation (1) (dashed trace). Note the deviation of the model from the experimental data (arrow). **(d)** Same data as in **(c)**, indentation $\delta$ *vs.* force $F$ with CoCS model fit, Equation (5). The experimental data is shown by the blue solid line and the fit by the dashed trace. The insets in **(a)** and **(c)** show confocal *z*-*x* profiles of beads (orange) on stiff and soft substrates (green). Scale bar: 10 μm. **(e)** Substrate deformability obtained from CoCS model fit with significantly higher deformability on soft compared to stiff substrates ($P = 0.012$, Wilcoxon-Mann-Whitney $U$ test). **(f)** Measured elastic moduli of beads on substrates of different stiffness obtained from Hertz fits (Equation (1), red) and CoCS model fits (Equation (5), blue). Note that the measured bead stiffness is independent of substrate stiffness when using the CoCS model fit ($P = 0.97$, Tukey test), as expected, but significantly depends on the substrate stiffness when using standard Hertz fits ($P = 0.008$, Tukey test). While they performed similarly well on stiff substrates ($P = 0.95$, Tukey test), on soft substrates the Hertz model yielded significantly lower bead elastic moduli when compared to the CoCS model fit ($P = 0.03$, Tukey test). Box plots show median (band),

quartiles (box), standard error (notches), and data points (dots); number of beads $N = 21$ and 39 for the soft and stiff substrates, respectively. * $P < 0.05$, ** $P < 0.01$.

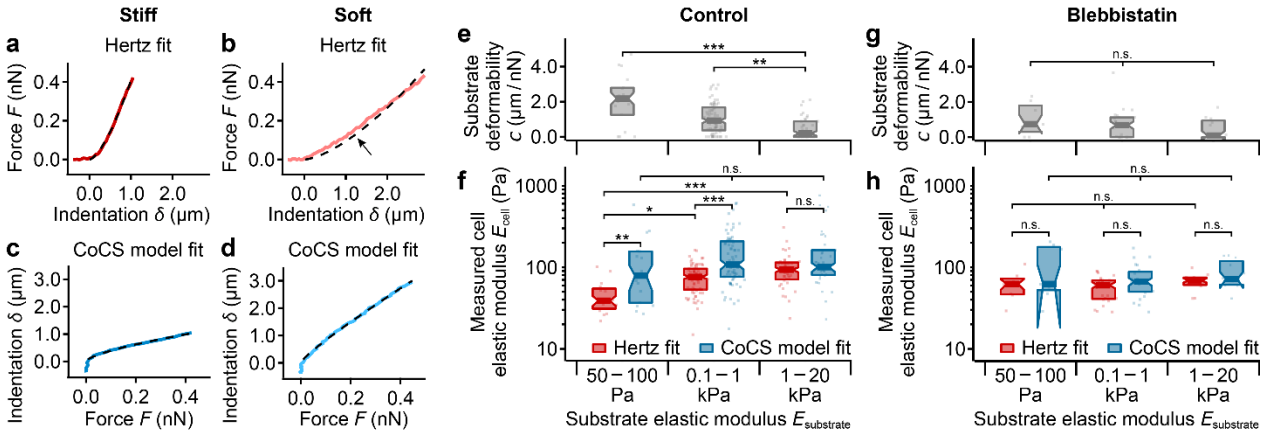


**Figure 5: Application to primary microglial cells. (a, b)** Representative force $F$ *vs.* measured indentation $\delta$ curves for cells on **(a)** stiff and **(b)** soft substrates with Hertz fits (Equation (1), dashed traces). As with beads (Figure 4), the Hertz model deviated from the experimental data when applied to cells grown on soft substrates (arrow). **(c, d)** Same data as in **(a, b)**, indentation $\delta$ *vs.* force $F$ on **(c)** stiff and **(d)** soft substrates with CoCS model fit (Equation (5), dashed traces). **(e)** Substrate deformability as a function of substrate stiffness obtained from CoCS model fits. Deformability increased significantly with decreasing substrate stiffness ($P \leq 0.004$, Kruskal Wallis ANOVA followed by Dunn-Holland-Wolfe posthoc test). **(f)** Apparent elastic moduli of live microglial cells on substrates of different stiffnesses as obtained from standard Hertz fits (Equation (1), red), and from CoCS model fits (Equation (5), blue). Similarly to PAA beads (Figure 4f), cells were significantly softer on soft and intermediate substrates when analyzed using standard Hertz fits ($P = 0.03$ and $P = 0.0006$, respectively, Tukey posthoc tests), but not when analyzed using the CoCS model fit ($P = 0.25$, one-way ANOVA). Compared to the Hertz model, the CoCS model yielded significantly larger cell stiffnesses on soft and intermediate substrates ($P = 0.0095$ and $4.0 \times 10^{-6}$, respectively, Tukey test), but a similar cell stiffness on stiff substrates ($P = 0.25$, Tukey test). **(g)** Substrate deformability and **(h)** apparent elastic moduli of microglial cells after treatment with the myosin-inhibitor blebbistatin on substrates of different stiffness. Deformability was similar on all substrates ($P = 0.6$, Kruskal-Wallis ANOVA), and the measured cell stiffness did not depend on substrate stiffness ($P \geq 0.3$, one way ANOVA) or on the fit model ($P \geq 0.1$, one way ANOVA followed by Tukey posthoc test). Box plots show median (band), quartiles (box), standard error (notches), and data points (dots); number of cells (e,f) $N = 17$, 74, and 39 and (g,h) $N = 7$, 24, and 12 for the soft, intermediate, and stiff substrates, respectively. * $P < 0.05$, ** $P < 0.01$, *** $P < 0.001$.

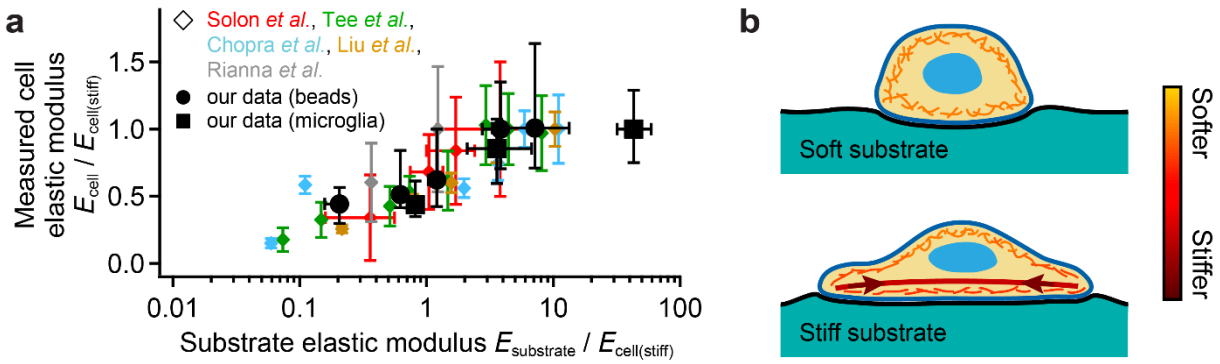


**Figure 6: Comparison of normalized published and current data analyzed by the Hertz model and hypothesis**. **(a)** Cell elastic moduli *vs.* substrate elastic moduli normalized by the respective cell elastic modulus on the stiffest gel used, $E_{\mathrm{cell(stiff)}}$. Note that data points collapse on a similar functional form. Data for various cell types from references[9-13] (diamond symbols) and data for beads and cells from this study (circles and squares, respectively). Data points and error bars represent average and standard deviation or median and quartiles, respectively. **(b)** Schematic of force propagation in cells cultured on deformable substrates. On soft substrates (top), traction forces are small. On stiffer substrates (bottom), traction forces (arrows) generated mostly be ventral stress fibers[45] (thick lines) increase with increasing substrate stiffness. These stress fibers undergo stress-stiffening and thus become stiffer with larger forces. These forces may be at least partly transmitted to the actomyosin cortex (thin fibers) but are dissipated with increasing distance from the stress fibers (illustrated by color going from red to orange). Hence, away from the stress fibers, the actin cortex does not stiffen significantly despite an increase in traction forces, as shown here by AFM measurements.